Traces in Proximity to Gaps in Return Planes

Theodore M. Zeeff, Todd H. Hubing, and Thomas P. Van Doren

***Abstract*—Coupling between circuitry on printed circuit boards can be mitigated by a variety of well-known techniques. One such technique is to isolate circuitry in different areas of the printed circuit board by strategically placing a gap in the signal return plane. However, this technique is only effective at reducing common-impedance coupling, which is generally not a significant coupling mechanism at frequencies above 1 MHz. This paper investigates the effect of a gap located between and parallel to adjacent microstrip traces. The effect of the gap on the mutual inductance and mutual capacitance is evaluated. Laboratory measurements and numerical simulations show that gaps in the return plane are ineffective at reducing inductive and capacitive crosstalk in most configurations, and in some cases they increase the mutual coupling between printed circuit board traces.**

***Index Terms*—Analog, common-impedance, coupling, digital, gapped, ground islands, ground plane, isolation, moating, mutual capacitance, mutual inductance, printed circuit board.**

I. Introduction

Coupling between parallel traces on the same printed circuit board, is due to one or more of the following coupling mechanisms: common-impedance, inductive or capacitive coupling. At low frequencies (e.g., below 100 kHz), common-impedance coupling tends to be the dominant coupling mechanism. At higher frequencies (e.g., above 1 MHz), inductive and capacitive coupling generally dominate. To reduce crosstalk between analog and digital circuitry, the EMC literature often recommends gapping the return plane between analog and digital areas on printed circuit boards [1], [2]. However, it is important to note that gapping the return plane in this manner is a technique for reducing common-impedance coupling and not inductive or capacitive coupling. Since common-impedance coupling is generally a low-frequency concern, gaps in the return plane are appropriate for solving or preventing low-frequency coupling problems. At frequencies above approximately 1 MHz however, gaps in a signal return plane can create more problems than they solve; particularly if they impede the flow of a signal current or if the voltage that develops across the gap drives a radiating structure [3].

This paper shows that at higher frequencies, gaps in a return plane are relatively ineffective at reducing the coupling between printed circuit board traces. In fact, they may enhance coupling by increasing the mutual inductance and capacitance between circuits even though none of the traces are routed over the gap. Laboratory measurements and computer simulations are used to support this conclusion.

II. General Equations for Coupling

Consider a microstrip trace geometry with the cross section shown in Fig. 1. The configuration consists of two traces of length l separated by an edge-to-edge distance s. Both traces have width w and are a height h above the return plane. These traces may be electrically coupled to one another by three mechanisms: a common impedance, mutual inductance and mutual capacitance. Fig. 2 shows a schematic of two circuits with all three coupling mechanisms represented. Circuit 1 is comprised of a source voltage V_s, a source resistance R_s, and a load resistance R_L. The susceptible circuit, Circuit 2, has near-end and far-end resistances $R_{\rm ne}$ and $R_{\rm fe}$, respectively. R_0 is the common impedance shared by both circuits.

The near-end and far-end coupling can be calculated using the following equations assuming $R_0 \ll R_L$, and $R_0 \ll R_s$ [1]

$$\frac{V_{\rm ne}}{V_s} = j\omega(M_{\rm ind\_}n + M_{\rm cap}) + M_{\rm ci\_}n \tag{1}$$

$$\frac{V_{\rm fe}}{V_s} = j\omega(M_{\rm ind\_}f + M_{\rm cap}) + M_{\rm ci\_}f \tag{2}$$

where $V_{\rm ne}$ and $V_{\rm fe}$ are the voltages coupled to near-end and far-end of Circuit 2, and

$$M_{\rm ci\_}n = \frac{R_{\rm ne}}{R_{\rm ne}+R_{\rm fe}}\frac{R_0}{R_s+R_L}$$

$$M_{\rm ci\_}f = \frac{R_{\rm fe}}{R_{\rm ne}+R_{\rm fe}}\frac{R_0}{R_s+R_L}$$

$$M_{\rm ind\_}f = \frac{R_{\rm fe}}{R_{\rm ne}+R_{\rm fe}}\frac{L_m}{R_s+R_L}$$

$$M_{\rm ind\_}n = \frac{R_{\rm ne}}{R_{\rm ne}+R_{\rm fe}}\frac{L_m}{R_s+R_L}$$

$$M_{\rm cap} = \frac{R_{\rm ne}\cdot R_{\rm fe}}{R_{\rm ne}+R_{\rm fe}}\frac{R_L\cdot C_m}{R_s+R_L}.$$

$M_{\rm ind}$ is directly proportional to the mutual inductance L_m between the two circuits. $M_{\rm cap}$ is directly proportional to the mutual capacitance C_m and $M_{\rm ci}$ is directly proportional to the resistance of the return plane R_0.

III. Equations for R_0 in a Microstrip Structure

At low frequencies, typically below a few kilohertz, the return current from a driven microstrip trace is uniformly distributed across the return plane and the value of R_0 can be computed as

$$R_0 = \frac{l}{\sigma_{\rm cu}\cdot w_{\rm plane}\cdot t_{\rm cu}} \tag{3}$$

where l is the length of the microstrip trace, $\sigma_{\rm cu}$ is the conductivity of the copper return plane, $w_{\rm plane}$ is the width of the return plane, and $t_{\rm cu}$ is the thickness of the copper. At frequencies where the skin depth δ is less than $t_{\rm cu}$, the equation below should be used in place of (3)

$$R_0 = \frac{l}{\sigma_{\rm cu}\cdot w_{\rm plane}\cdot \delta} \tag{4}$$

where δ is defined as

$$\delta = \frac{1}{\sqrt{\pi\cdot f\cdot \mu\cdot \sigma_{\rm cu}}}. \tag{5}$$

However, when the resistance of the return plane is significantly lower than the branch inductive reactance of the return plane, typically at frequencies above a few megahertz, the return current is not evenly distributed over the surface of the plane [4], and the current distribution is more accurately described by [5]

$$K(x) = \frac{I_s}{\pi}\cdot\left[\frac{1}{w}\cdot\left(\tan^{-1}\left(\frac{x+\frac{w}{2}}{h}\right)-\tan^{-1}\left(\frac{x-\frac{w}{2}}{h}\right)\right) + \frac{4h}{w_{\rm plane}\cdot\pi}\cdot\frac{1}{\sqrt{\left(\frac{w_{\rm plane}}{2}\right)^2-x^2}}\right] \tag{6}$$

where x is the distance from the center of the source trace, and I_s is the magnitude of the total current flowing on the source trace. The current

Manuscript received July 1, 2002; revised September 17, 2004.

T. M. Zeeff is with Hewlett-Packard Company, San Diego, CA 92127 USA.

T. H. Hubing and T. P. Van Doren are with the Department of Electrical and Computer Engineering, University of Missouri-Rolla, Rolla, MO 65409 USA (e-mail: hubing@umr.edu).

Digital Object Identifier 10.1109/TEMC.2005.847405

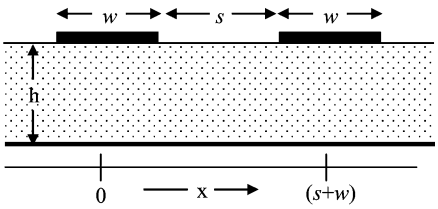

Fig. 1. Cross section of the coupled microstrip trace pair.

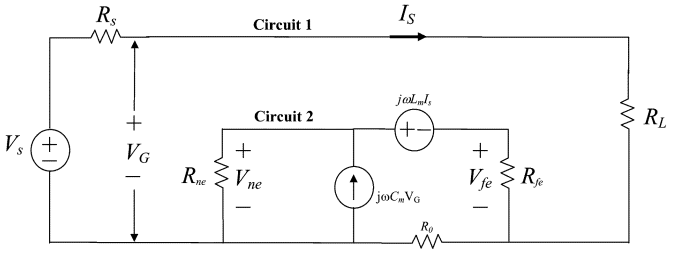

Fig. 2. Schematic of two mutually coupled circuits.

distribution $K(x)$ (for $I_s = 1$ Ap, $w = 45$ mil, $h = 45$ mil, and $w_{\text{plane}} = 8000$ mil) is shown in Fig. 3. Using this current distribution, the common resistance R_0 can be computed as

$$R_0(x) = \frac{K(x) \cdot l}{I_s \cdot \delta \cdot \sigma_{\text{cu}}}. \tag{7}$$

Note how R_0, and, therefore, the common-impedance coupling, decreases the farther the coupled trace is from the source trace.

IV. Measurements and Simulations

A. Laboratory Measurements

Laboratory measurements employed a network analyzer to measure the coupling between two microstrip trace circuits. The measured coupling was then used to derive expressions for mutual inductance and mutual capacitance. The test board geometry used for the laboratory measurements is illustrated in Fig. 4. Each test board had a pair of parallel microstrip traces. Each microstrip trace had SMA connectors on each end. The properties of the test boards were as follows: $w = 0.114$ cm (45 mil), $\varepsilon_r = 4.3, h = 0.114$ cm (45 mil) and $l = 10$ cm. The separation between the traces was $s = 0.381$ cm (150 mil) or $s = 0.114$ cm (45 mil) depending on the measurement. A network analyzer was used to measure the voltage transfer coeffient S_{21} between Port 1 connected to one microstrip trace and Port 2 attached alternately to the near-end and far-end of the other microstrip trace. To measure mutual capacitance, both traces were terminated with an open circuit. To measure mutual inductance, both traces were terminated with a short. Near-end and far-end crosstalk measurements were made from 0.03 MHz to 1 GHz. The mutual inductance and mutual capacitance were determined from S_{21} as [6]

$$C_m = \frac{|S_{21}|}{2 \cdot \omega \cdot Z_L \cdot l} \tag{8}$$

$$L_m = \frac{|S_{21}| \cdot Z_L}{2 \cdot \omega \cdot l} \tag{9}$$

where Z_L is the port impedance of the network analyzer. In order to obtain the most accurate values for L_m and C_m, the values of S_{21} were determined at 2 MHz where the magnitude of S_{21} increased at a rate of 20 dB/decade.

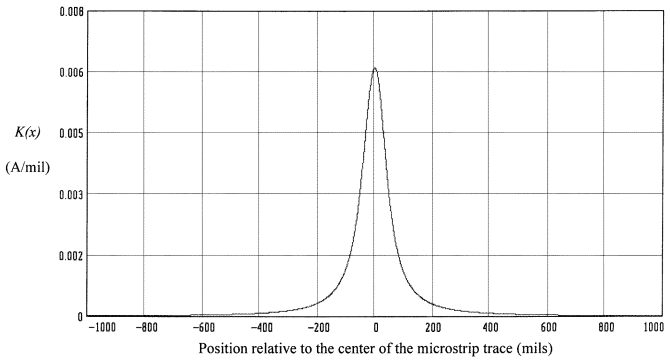

Fig. 3.Current distribution across the return plane for a microstrip trace plotted as a function of the distance from the center of the microstrip trace.

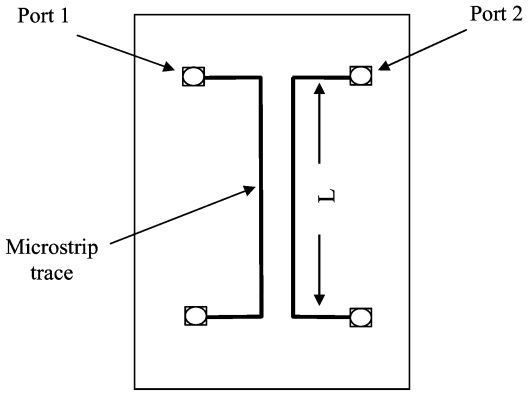

Fig. 4. Top view of the test board used in measurements.

B. Numerical Simulations

Two-dimensional (2-D) and three-dimensional (3-D) numerical simulations were performed using a commercially available, FEM-based software package [7]. The 2-D simulations solved for L_m and C_m per unit length directly, while the 3-D simulations calculated S-parameters from which the coupling parameters were determined using (8) and (9).

V. Coupling Without a Gap in the Return Plane

The measured $|S_{21}|$, shown in Fig. 5, can be broken into three frequency ranges. In the inductive coupling measurement, from 30 kHz to roughly 100 kHz, the dominant coupling mechanism is common-impedance coupling. There is no measurable common-impedance coupling in the capacitive coupling measurement due to the open-circuit termination. From 300 kHz to 30 MHz, the principal coupling mechanism in both measurements is either mutual inductance or mutual capacitance. At frequencies above 30 MHz, the length of the microstrip trace is no longer short relative to a wavelength and the $|S_{21}|$ curve exhibits transmission line effects.

Values of mutual capacitance and mutual inductance derived from the measurements are compared to values derived from the 2-D numerical modeling in Table I. The numerical results agree with the measured results within 1.4 dB (16%).

VI. Coupling With a Gap in the Return Plane

Common-impedance coupling requires the source circuit and the victim circuit to share parts of their signal current path. At low frequencies, where common-impedance coupling is dominant, cutting a gap in the plane between the traces can effectively isolate the source circuit from the victim circuit and reduce the coupling. However, at higher frequencies where inductive or capacitive coupling is dominant,

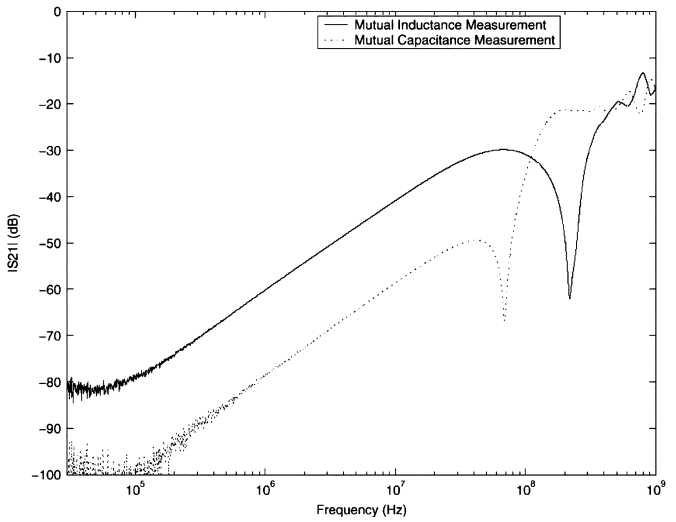

Fig. 5. Network analyzer measurements of S_{21} between two microstrip traces.

TABLE I
COMPARISON BETWEEN THE VALUES OF MUTUAL INDUCTANCE AND MUTUAL CAPACITANCE DERIVED FROM MEASUREMENTS (AT 2 MHz) AND NUMERICAL SIMULATIONS

Trace Separation, s	L_m (nH/m)		C_m (pF/m)	
	Measurements	FEM Solution	Measurements	FEM Solution
0.114 cm	68.5	78.7	10.9	9.20
0.381 cm	20.2	20.7	0.984	1.10

gapping the return plane in this manner is generally ineffective and may actually increase coupling.

A. Capacitive Coupling With a Gap in the Return Plane

A gap was cut parallel to and in between the coupled microstrip traces on the test board. A cross section of the microstrip trace pair with a gap in the return plane is shown in Fig. 6. The gap ran the entire length of the test board. For this test board, $l = 19$ cm, and $s = 0.381$ cm (150 mil). The width of the gap $w_{\rm gap}$ was varied from 0 cm (no gap) to 0.381 cm (150 mil). In addition to the measurements, 2-D FEM-based software was used to investigate the effects of the gap. The data from the measurements and simulations is summarized in Table II.

The data in Table II shows that the mutual capacitance increases slightly when a narrow gap is introduced into the return plane. The change in the mutual capacitance becomes substantial when $w_{\rm gap}$ is on the order of the separation between the microstrip traces s. When a gap is cut into the return plane, part of the return plane is removed and more of the electric flux that would normally couple to the return plane from the source trace couples to the victim trace, thereby increasing mutual capacitance.

B. Inductive Coupling With a Gap in the Return Plane

1) Effects of the Gap Length: To measure the effect of a gap in the return plane on inductive coupling, a gap was cut parallel to and in the middle of the microstrip trace pair. The gap was first introduced in the middle of the return plane and was lengthened by short increments until the gap reached the edges of the test board. Fig. 7 illustrates how the gap was introduced into the ground plane and Fig. 8 shows the measured results. For the test board used in this experiment, $s = 0.381$ cm (150 mil) and $w_{\rm gap} = 0.0254$ cm (10 mil).

Fig. 8 shows that the inductive coupling increases as the length of the gap, l, is lengthened. When the gap extends beyond the coupled

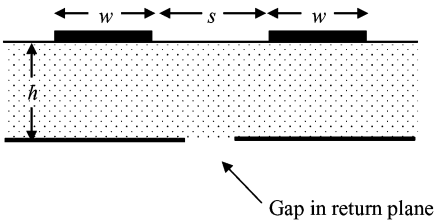

Fig. 6. Cross section of coupled microstrip traces with a gap in the return plane.

TABLE II
FEM-BASED SOLUTIONS AND MEASURED VALUES OF MUTUAL CAPACITANCE WITH A GAP IN THE RETURN PLANE

Gap Width	C_m (pF/m)	
	Measurements	FEM Solution
0.381 cm	3.794	3.705
0.305 cm	2.578	2.528
0.254 cm	1.881	1.985
0.127 cm	1.346	1.161
0.076 cm	1.143	1.156
0.025 cm	-	1.104
0 cm	0.984	1.098

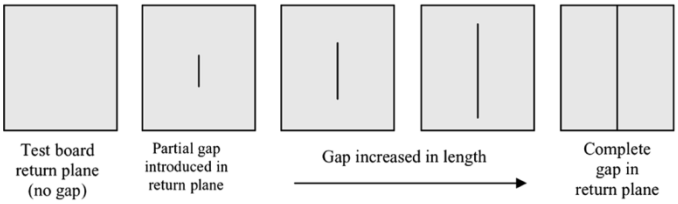

Fig. 7. Return plane of the test boards is shown. A gap in the return plane is introduced in the middle of the board. The gap is lengthened until the gap reaches the entire span of the test board.

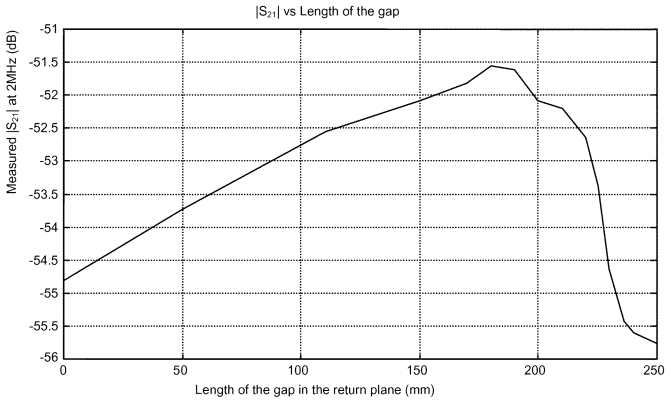

Fig. 8. $|S_{21}|$ for inductive crosstalk as a function of the length of the gap in the return plane. The test board was 250 mm long and the length of the coupled traces was 190 mm.

length of the traces (190 mm), inductive coupling decreases until the gap approaches the edges of the test board (complete gap). The measured inductive coupling with a complete gap, shown in Fig. 8, is approximately 1 dB less than it is with no gap in the return plane. Also, the inductive coupling reaches a maximum when $l_{\rm gap} = 1$.

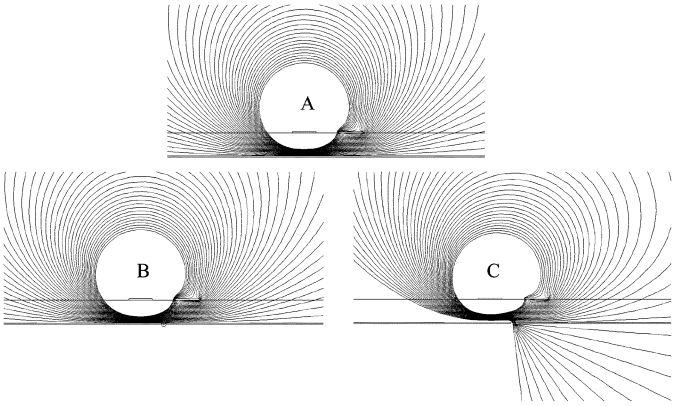

Fig. 9. Contour plots of the magnetic flux for a test board with (A) no gap, (B) a partial gap, and (C) a complete gap in the return plane. $s = 0.114$ cm.

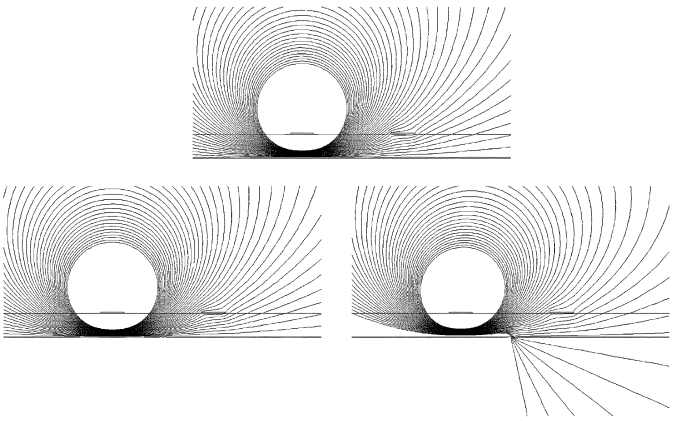

Fig. 10. Contour plots of the magnetic flux for a test board with (A) no gap, (B) a partial gap, and (C) a complete gap in the return plane. $s = 0.381$ cm.

TABLE III
COMPARISON BETWEEN THE VALUES OF MUTUAL INDUCTANCE DERIVED FROM MEASUREMENTS AND NUMERICAL SIMULATIONS FOR THREE DIFFERENT TEST BOARDS

s = 0.114 cm	L_m (nH/m)		
	No Gap ($l_{gap} = 0$)	Complete Gap ($l_{gap} = l_{board}$)	Partial Gap ($l_{gap} = l$)
Measurements	68.5	54.2	69.0
2-D Simulations	78.7	62.0	78.9
3-D Simulations	86.1	71.7	86.1
s = 0.381 cm	L_m (nH/m)		
	No Gap ($l_{gap} = 0$)	Complete Gap ($l_{gap} = l_{board}$)	Partial Gap ($l_{gap} = l$)
Measurements	20.0	14.9	20.0
2-D Simulations	20.7	15.9	20.7
3-D Simulations	20.8	18.5	20.8

TABLE IV
FEM-BASED SOLUTIONS AND MEASURED VALUES OF MUTUAL INDUCTANCE WITH A COMPLETE GAP IN THE RETURN PLANE

Gap Width	L_m (nH/m) (s = 0.381 cm)	
	Measurements	FEM Solution
0.381 cm	19.45	21.67
0.305 cm	16.48	18.46
0.254 cm	15.13	16.95
0.127 cm	14.29	15.27
0. 076 cm	14.35	15.30
0.025 cm	-	15.87
0 cm	20.18	20.68

To better understand the fundamental mechanism at work, an analysis was performed using 2-D and 3-D numerical tools. Inductive coupling was evaluated under three conditions; a test board with no gap ($l_{\rm gap} = 0$), a test board with a partial gap ($l_{\rm gap} = l$), and a test board with a complete gap ($l_{\rm gap} = l_{\rm board}$).

Two test boards, one with $s = 0.381$ cm (150 mil) and the other with $s = 0.114$ cm (45 mil) were simulated with the 2-D software tool. In both cases, $w_{\rm gap} = 0.0254$ cm (10 mil). For the partial gap case, the boundary conditions in the software were set to allow current to return on both sides of the gap. For the full gap case, current was forced to return on the source side of the gap. Contour maps of the magnetic flux for each test configuration are shown in Figs. 9 and 10. The highest valued contour line in each of the contour plots is the line that is closest to the source trace, which is the left-most trace in each figure. Contour lines nearest the source trace were omitted for ease of viewing. Each contour plot uses the same scale. Computed values of L_m are provided in Table III along with measured results.

As shown in the contour maps of the flux in Figs. 9 and 10, a partial and narrow gap in the return plane has little or no effect on the magnetic flux. The magnetic flux does not change because the return current is allowed to flow where it did before the gap was cut into the return plane. In the case with a complete and narrow gap, the return current is forced to flow only on the side of the return plane directly beneath the source trace and the magnetic flux near the victim trace is changed. Figs. 9(c) and 10(c) show that the complete gap allows some flux to wrap the return plane of the susceptible circuit. The magnetic flux passing between the victim trace and the return plane in this case is slightly less ($\sim$2 dB) than it was with no gap in the return plane.

The primary difference between a partial gap and a complete gap in the return plane is where the return current is allowed to flow. With a partial and narrow gap in the return plane, like that in Figs. 9 and 10, the return current is allowed to spread out across the return plane just as it was able to do when there was a solid return plane. Since the gap width is very small, the return current is not disrupted and the mutual inductance is not affected. However, when the return current is restricted to the side under the source trace, the magnetic flux pattern is changed and the magnetic flux coupling the victim circuit decreases.

To substantiate the results found in the 2-D analysis of the test boards, a 3-D software tool was used to simulate each of the three test board configurations. The results of the 3-D analysis are also shown in Table III.

2) Effects of the Gap Width: To measure the effect of the gap width on mutual inductance, the width of a complete gap in the test boards was varied. The width of the gap ranged from 0 cm (no gap) to 0.381 cm (150 mil). The edge-to-edge trace separation for the test board was 0.381 cm (150 mil). The results from the measurements and 2-D simulations are provided in Table IV. Contour maps of the magnetic flux are provided in Fig. 11 for many of the gap widths tested. The data in Table IV shows that wider gaps can actually increase the mutual inductance. However, the increase in mutual inductance only becomes significant when the width of the gap $w_{\rm gap}$ is on the order of the trace separation s.

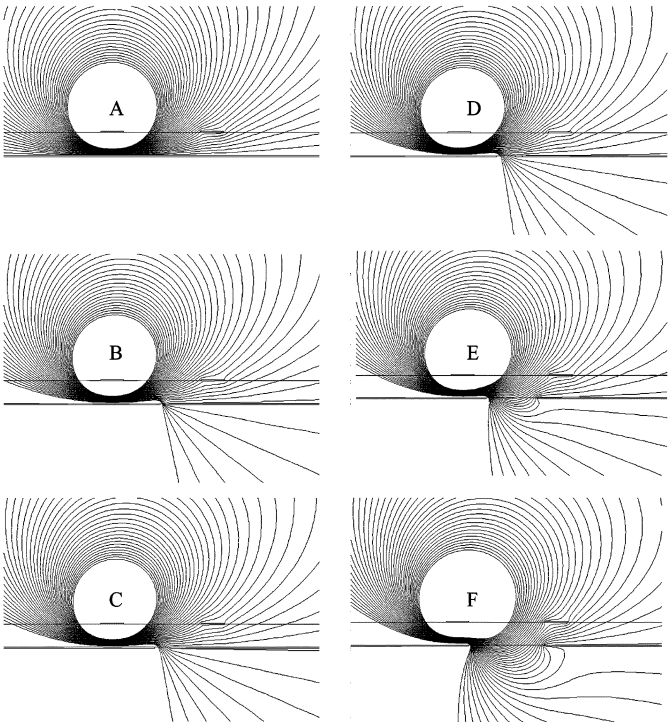

Fig. 11. Contour maps of the magnetic flux from test boards with varying width gaps in the return plane. (a) No gap. (b) $w_{gap} = 0.025$ cm. (c) $w_{gap} = 0.076$ cm. (d) $w_{gap} = 0.127$ cm. (e) $w_{gap} = 0.305$ cm. (f) $w_{gap} = 0.381$ cm.

VII. Conclusion

Gapping the return plane is an effective way to reduce or even eliminate common-impedance coupling between two parallel microstrip traces. However, a gap cut into the return plane has been shown to be ineffective at reducing capacitive and inductive coupling.

For capacitive coupling, experiments have shown that adding a gap in the return plane actually increases the mutual capacitance. However, the change is rather insignificant unless the width of the gap is quite large.

Two factors determine the effect of the gap on inductive coupling, the length of the gap and the width of the gap. Experiments show that if the gap is long enough to prevent current from flowing underneath the victim trace, then the mutual inductance may decrease slightly ($\sim$2 dB). When the gap is widened, there is a slight increase in inductive coupling. However overall, the gap has relatively little effect on inductive coupling.

To reduce crosstalk between circuits on a printed circuit board at frequencies below a few hundred kilohertz, where common-impedance coupling is likely to dominate, it may be advisable to gap the current return plane. However, gapping the return plane is not likely to reduce crosstalk at frequencies above a few hundred kilohertz where inductive and capacitive coupling dominate.

References

[1] C. R. Paul, *Introduction to Electromagnetic Compatibility*. New York: Wiley, 1992.

[2] C. Christopoulos, *Principles and Techniques of Electromagnetic Compatibility*. Boca Raton, FL: CRC, 1995, pp. 221–245.

[3] B. Archambeault, "Proper design of intentional splits in the ground reference plane of PC boards to minimize emissions on I/O wires and cables,," in *Proc. Int. Symp. Electromagnetic Compatibility*, Denver, CO, Aug. 1998, pp. 768–773.

[4] D. M. Hockanson, J. L. Drewniak, T. H. Hubing, T. P. Van Doren, F. Sha, C. W. Lam, and L. Rubin, "Quantifying EMI resulting from finite-impedance reference planes," *IEEE Trans. Electromagn. Compat.*, vol. 39, no. 3, pp. 225–232, Aug. 1997.

[5] C. L. Holloway and E. F. Kuester, "Net and partial inductance of a microstrip ground plane," *IEEE Trans. Electromagn. Compat.*, vol. 40, no. 1, pp. 33–46, Feb. 1998.

[6] W. Cui, H. Shi, X. Luo, J. L. Drewniak, T. P. Van Doren, and T. Anderson, "Lumped-element sections for modeling coupling between high-speed digital and I/O lines," in *Proc. Int. Symp. Electromagnetic Compatibility*, Austin, TX, Aug. 1997, pp. 260–265.

[7] Maxwell 2-D Extractor Ver. 4.0.04 and Ansoft HFSS Ver 6.0, Ansoft Corporation, Pittsburgh, PA, 1998.

Wide-Band Lorentzian Media in the FDTD Algorithm

Marina Y. Koledintseva, James L. Drewniak, David J. Pommerenke, Giulio Antonini, Antonio Orlandi, and Konstantin N. Rozanov

***Abstract*—This paper considers the case of a wide-band Lorentzian (WBL) algorithm in the finite-difference time-domain (FDTD) modeling of dispersive media. It is shown herein that the WBL model is a physically meaningful and practically useful case of the frequency behavior of materials along with the Debye and narrow-band Lorentzian (NBL). The recursive convolution algorithms for the finite-difference time-domain technique for NBL and WBL models differ. The Debye model, which is suitable for comparatively low-frequency dispersive materials, may not have sufficient number of parameters for describing the wide-band material, especially if this material exhibits pronounced absorption at higher frequencies. It is shown that the Debye model can be used, if the Q-factor of the linear circuit analog corresponding to the Lorentzian model of the material is less than approximately 0.8. If the quality factor is in the limits of about $0.8 < Q \leq 1$, then the WBL model is appropriate. For $Q > 1$, the NBL model must be applied. The NBL model is suitable for dielectrics exhibiting resonance effects in the microwave frequency range. The WBL model is typical for composites filled with conducting fibers.**

***Index Terms*—Debye model, dispersive media, finite-difference time-domain (FDTD) technique, Lorentzian model, recursive convolution.**

I. Introduction

The finite-difference time-domain (FDTD) method applied to the analysis of complex electromagnetic structures, including those containing dispersive composite dielectric, magnetic, and magnetodielectric media, has become widespread because of its robustness and comparative simplicity [1]–[3]. It is known that for linear dispersive media, the linear recursive convolution (LRC) approach is computationally effective, straightforward to implement and, therefore, attractive [1]–[4]. To implement the LRC or piecewise linear recursive convolution (PLRC) procedure, the frequency dependence of the material dielectric or magnetic susceptibility must be a rational function

Manuscript received February 9, 2004; revised August 28, 2004.

M. Y. Koledintseva, J. L. Drewniak, and D. J. Pommerenke are with the EMC Laboratory, University of Missouri, Rolla, MO 65409 USA (e-mail: marinak@umr.edu).

G. Antonini and A. Orlandi are with the Department of Electrical Engineering, University of L'Aquila, Poggio di Roio, 67040 AQ, Italy (e-mail: antonini@ing.univaq.it).

K. N. Rozanov is with the Microwave Laboratory of the Institute for the Theoretical and Applied Electromagnetics, Russian Academy of Sciences, 125412 Moscow, Russia (e-mail: k_rozanov@mail.ru).

Digital Object Identifier 10.1109/TEMC.2005.847406